ARTICLES

Thermal Evolution of Transitional Aluminas Followed by NMR and IR Spectroscopies

C. Pecharromán,* I. Sobrados, J. E. Iglesias, T. González-Carreño, and J. Sanz

Instituto de Ciencia de Materiales, Consejo Superior de Investigaciones Cientificas, Cantoblanco 28049, Madrid, Spain

Received: August 7, 1998; In Final Form: May 10, 1999

Thermal decomposition of boehmite and bayerite has been studied by X-ray diffraction and by NMR and IR spectroscopies. Coordination and site distortion of Al polyhedra have been estimated by ^{27}Al NMR spectroscopy while IR optical properties of transitional aluminas, η-, γ-, δ-, and θ-Al_2O_3 were derived from IR near-normal specular reflectance technique. In the low-temperature phases, aluminum vacancies are located in tetrahedral positions in γ-Al_2O_3 while in η-Al_2O_3 they are distributed at random between tetrahedral and octahedral positions. In addition, a small amount (5%) of pentahedrally coordinated aluminum was found in γ-alumina, which has been tentatively assigned to Al at the external surface of alumina particles. At 800 °C a notable increase in structural ordering was detected in both phases; in the case of η-Al_2O_3, this change accelerates the continuous transformation into θ-Al_2O_3 which is totally achieved at 1000 °C. On the contrary, γ-Al_2O_3, does not show any sign of transformation until 900 °C; at 950 °C pentahedral cations disappear and formation of θ-Al_2O_3 is detected by IR and NMR techniques. From 900 to 1200 °C, γ-, θ-, and α-Al_2O_3 coexist in samples obtained from boehmite. Above 1200 °C corundum is the only thermodynamically stable phase in both series of samples.

Introduction

Corundum α-Al_2O_3 is the ultimate product of hydroxides, oxyhydroxides, and oxides of aluminum heated at high temperatures. In addition to α-Al_2O_3, several materials, known as transition aluminas, can be metastably obtained in the laboratory and industry during dehydration of tryhydrates $Al(OH)_3$ (bayerite and gibbsite) and monohydrates AlOOH (boehmite and diaspore). The nature of a transitional alumina strongly depends on its precursor; thus, thermal decomposition of bayerite gives the sequence $\eta \rightarrow \theta \rightarrow \alpha$, while that of boehmite gives $\gamma \rightarrow \delta \rightarrow \theta \rightarrow \alpha$. An extensive review about all different aluminum oxides, hydroxides and oxyhydroxides, and their transformations can be found in ref 1.

Dehydroxylation reactions preserve the skeleton of the parent material[2] while OH^- groups are eliminated. If the oxygen network of the precursor is close to fcc (boehmite and bayerite), heating treatments produce spinel-like materials.[2−7] γ- and η-Al_2O_3 are always obtained with small crystallite size and their X-ray powder diffraction patterns, showing broad reflections, correspond to cation-defective spinels (Megaw,[8] Greenwood,[9] Zhou and Snyder[4]). The ideal structure of these phases belongs to space group $Fd\bar{3}m$, but their real structure seems to be tetragonally distorted.[1,2,10] Distortions are different in both phases and they have been associated with differences in cation ordering. From ^{27}Al MAS-NMR data,[3] cation vacancies have been reported to be restricted to tetrahedral sites in γ-Al_2O_3 and to octahedral sites in η-Al_2O_3; however, after Rietveld analyses of neutron diffractograms, cation distribution was different.[4] At present, it is admitted that cation ordering increases with the temperature of treatment, but the structural features of transitional aluminas are not yet well-known. In the case of θ-Al_2O_3, the highest term of the bayerite and boehmite series, the oxygen network makes up a distorted fcc lattice complex, but the octahedral and tetrahedral aluminum distribution violates the 4-fold symmetry rotation axis of the spinel space group.[4−6] In this monoclinic structure the relative amounts of tetrahedral and octahedral aluminum are 50−50%. The formation temperature of this phase depends on the precursor and it can be very close to that of corundum. The transformation from transitional aluminas to α-Al_2O_3, with a hexagonal oxygen sublattice in which all Al are octahedrally coordinated,[8] occurs through a nucleation and growth process.[10]

The main objective of this article is the determination of structural properties of transition aluminas. ^{27}Al MAS-NMR and reflectance IR spectroscopies as well as X-ray diffraction have been used to monitor structural transformations produced during the thermal heating of bohemite and bayerite. From MAS-NMR data, evolution of the coordination of aluminum and distortions of polyhedra have been analyzed. IR specular reflectance spectroscopy has been used to determine vibrational modes (frequencies, intensities, and damping constants) which are strongly dependent on the crystal structure of alumina phases. In previous works, the IR optical properties of η-Al_2O_3[11] and the low-resolution NMR spectra of γ-Al_2O_3[12] have been reported. In this article, a more accurate and systematic study of dehydroxylation and further thermal transformations of bayerite and boehmite has been undertaken by simultaneous analysis of data from both spectroscopies.

* To whom all correspondence should be addressed. E-mail: cpg@icmm.csic.es.

10.1021/jp983316q CCC: $18.00
Published on Web 07/13/1999

Sample Synthesis Procedure

Two different kinds of aluminas have been studied at different stages of thermal treatment. The first series of data was obtained by thermal treatment of separate bayerite (Condea) samples, heated for 2 h at 300, 500, 700, 800, 900, and 1000 °C. In the second case, a γ-Al_2O_3 sample (Girdler) with a specific surface of 208 m^2/g, obtained from dehydroxylation of boehmite at 600 °C was used. This sample was accumulatively calcined at increasing temperatures for periods of 2 h up to 1200 °C. Several amounts of the original γ-Al_2O_3 sample were fired at 1200 °C for short periods of time (several minutes) to increase the proportion of θ phase.[10] After each treatment, the samples were checked by XRD to follow structural changes.

Experimental and Data Treatment

X-ray Diffraction. X-Ray diffraction powder patterns of samples were recorded with a PW1050/25 Philips diffractometer fitted with an automatic divergence slit, a diffracted beam curved graphite monochromator (Cu K_α radiation), a 0.07° receiving slit and a proportional detector. Data were collected in the 2θ range 10−70°, with a scanning rate of 2.4°/min.

IR Spectroscopy. For IR reflectance analyses, powders were compacted in an uniaxial press under a nominal pressure of 1 GPa. A very smooth die, made in zirconia partially stabilized with yttria, was used to obtain self-supporting powder pellets with a good quality specular surface. The IR spectra were taken in a Nicolet 20 SXC FTIR spectrophotometer, from 4000 to 220 cm^{-1}, sampling every 0.48 cm^{-1}, in a near-normal specular reflectance experimental setup.

IR reflectance spectra of the powder aggregates can be used to determine the IR complex dielectric constant. In this respect, reflectance measurements have advantages in comparison with more common absorbance experiments: they are quantitative, they do not depend on the preparation method, and they weight in the same way low- and high-frequency data. In most of the previously published IR absorbance spectra, low-frequency bands (from 200 to 500 cm^{-1}) are either missing or else they display a very poor intensity. In addition, by using an effective medium approximation, it is possible to accurately reproduce the experimental reflectance of the powder pellet by calculation, and hence deduce its intrinsic IR optical parameters.

The normal specular reflectance is related to the dielectric constant through one of the Fresnel equations:

$$R = \left|\frac{(\sqrt{\langle\epsilon\rangle} - 1)}{(\sqrt{\langle\epsilon\rangle} + 1)}\right|^2 \tag{1}$$

where $\langle\epsilon\rangle$ is the average dielectric constant of the aggregate, defined as

$$\langle\epsilon\rangle = \frac{\int_V D(\vec{r})\,dV}{\epsilon_0 \int_V E(\vec{r})\,dV} = \frac{\int_{V_m} \epsilon_m(\vec{r}) E_m(\vec{r})\,dV + \int_{V_p} \epsilon_p(\vec{r}) E_p(\vec{r})\,dV}{\int_{V_m} E_m(\vec{r})\,dV + \int_{V_p} E_p(\vec{r})\,dV} \tag{2}$$

We suppose that this aggregate is composed by a mixture of isotropic spheroidal powder ("p" subscript) and spheroidal matrix ("m" subscript) particles. In this case the matrix is air. Under these approximations and introducing an "effective medium" hypothesis,[13,14] the average dielectric constant can be calculated[15,16] as

$$\langle\epsilon\rangle = \left\{(1-f)\epsilon_m\left[\frac{2}{(1-L_m)\langle\epsilon\rangle + L_m\epsilon_m} + \frac{1}{2L_m\langle\epsilon\rangle + (1-2L_m)\epsilon_m}\right] + f\left[\frac{2\epsilon_p}{(1-L_p)\langle\epsilon\rangle + L_p\epsilon_p} + \frac{\epsilon_p}{2L_p\langle\epsilon\rangle + (1-2L_p)\epsilon_p}\right]\right\} \Big/ \left\{(1-f)\left[\frac{2}{(1-L_m)\langle\epsilon\rangle + L_m\epsilon_m} + \frac{1}{2L_m\langle\epsilon\rangle + (1-2L_m)\epsilon_m}\right] + f\left[\frac{2}{(1-L_p)\langle\epsilon\rangle + L_p\epsilon_p} + \frac{1}{2L_p\langle\epsilon\rangle + (1-2L_p)\epsilon_p}\right]\right\} \tag{3}$$

To solve this equation in $\langle\epsilon\rangle$, it is necessary to know f, the filling factor, L_p, and L_m, the depolarization factors of particles and matrix; and ϵ_p, the dielectric constant of the particles. The filling factor can be directly measured by weighing the pellet. The geometric factors L_p and L_m,[17] are related to the particle shape and the percolation f_c threshold.[15] In our case, the particles have irregular shape but they can approximately be taken as spheres. In the case of spheres, the value of depolarization factor is $L_p = {}^1/_3$. Finally, for ϵ_p, a superposition of harmonic oscillators[11,18−20] is assumed.

$$\epsilon_p = \epsilon_\infty \prod_{k=1}^{N} \frac{\omega_{Lk}^2 - \omega^2 - i\gamma_{Lk}\omega}{\omega_{Tk}^2 - \omega^2 - i\gamma_{Tk}\omega} \tag{4}$$

where k runs over the vibrational modes, ϵ_∞ is the dielectric constant at optical frequencies, ω_{Tk} and ω_{Lk} are the transverse and longitudinal frequencies, and γ_{Tk} and γ_{Lk} are the decay ratio or damping constant frequencies of the kth mode. In the dielectric constant function, poles and zeros correspond to transverse and longitudinal frequencies so high reflectance bands extend from ω_{Tk} to ω_{Lk} and the intensity mainly depends on γ_{Tk} and γ_{Lk}. The previous considerations apply to perfect crystals. In most of our samples the crystallinity is very poor so that the selection rules relax and the maxima of dielectric function broaden. Even in these conditions the dielectric constant can be fitted by eq 4. However, the damping parameters γ_{Tk} and γ_{Lk} do not only represent the decay ratio but also the broadening of the imaginary part of the dielectric function due to the lack of crystallinity. In this paper we have fitted these parameters from experimental spectra and by analogy we have called them damping parameters. This is an usual convention among researchers dealing with optical properties of powdered materials,[21−23] although it is clear that this use does not properly conform to the physical concept of damping.

Using eqs 1, 3, and 4 it is possible to calculate the reflectance as a function of the parameters f, f_c, ϵ_∞, ω_{Tk}, γ_{Tk}, ω_{Lk}, and γ_{Lk}. Only the filling factor is experimentally fixed, while the rest are adjusted by a nonlinear least-squares refinement. The starting value for ϵ_∞ is obtained from the reflectance in the IR transparency region (4000−1200 cm^{-1}), and the percolation threshold is assumed to be $f_c \cong 0.9f$. Initial values of the remaining parameters are judiciously chosen. The goodness of the fit is judged from the estimator.

$$R = \left[\frac{\sum (R_{th} - R_{exp})^2}{\sum R_{exp}^2}\right]^{1/2} \tag{5}$$

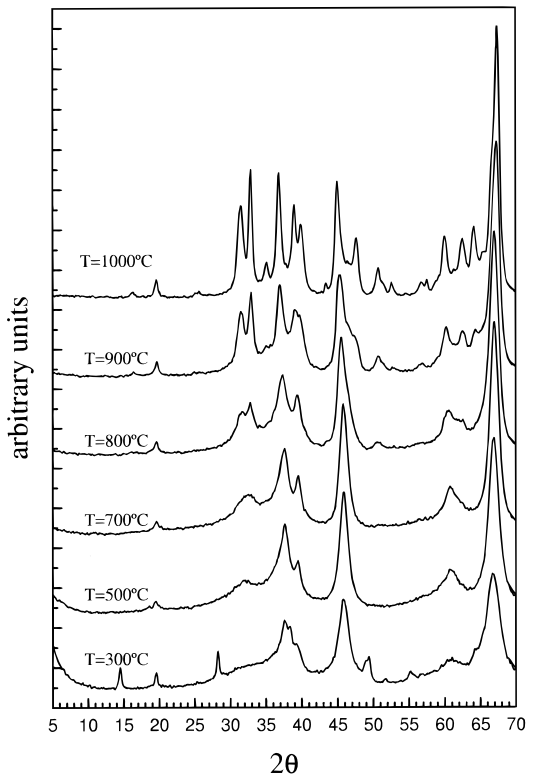

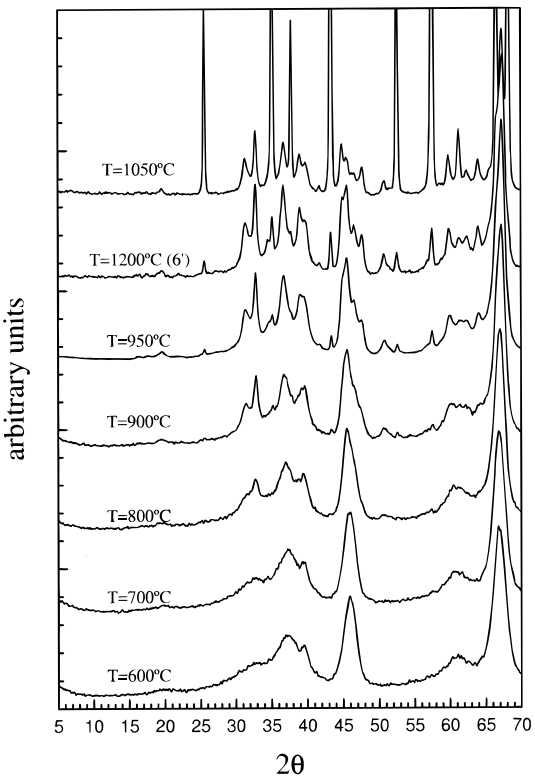

Figure 1. XRD powder patterns obtained from thermal evolution of (a, top) transitional aluminas obtained from bayerite samples (α-Al-$(OH)_3$) taken for the same initial batch, heated for 2 h at the specified temperatures (initial bayerite diffractogram not shown); (b, bottom) transitional aluminas obtained from an original sample of γ-Al_2O_3 prepared from bohemite (γ-AlOOH) after dehydroxylation at 600 °C and subjected to accumulative thermal treatments of 2 hours at the indicated temperatures. The pattern labeled as "T = 1200 °C (6′)" corresponds to the original sample heated for only 6 min at 1200 °C.

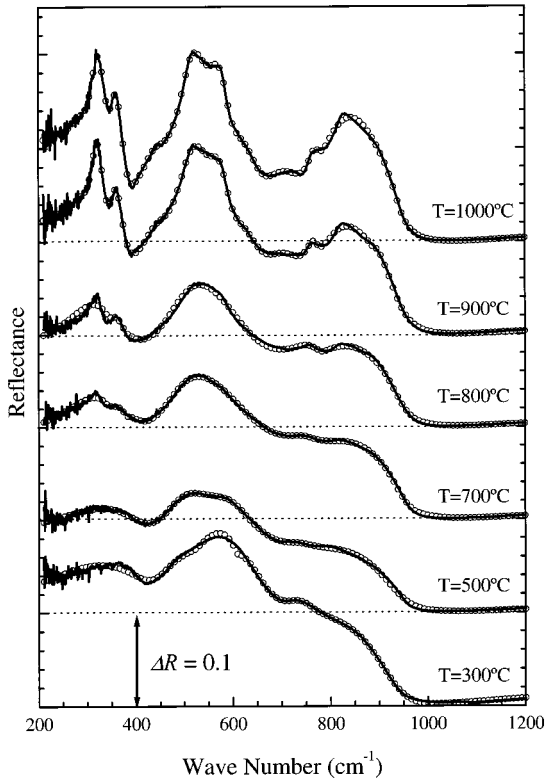

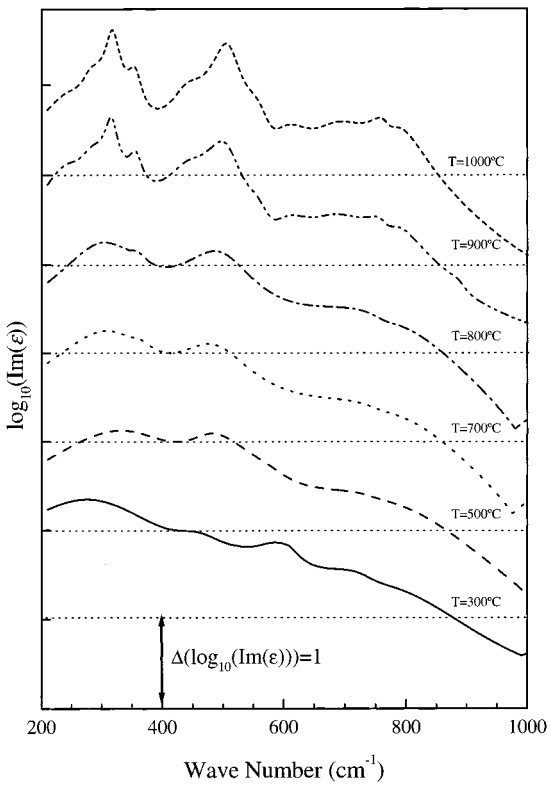

Figure 2. (a, top) Experimental IR reflectance spectra (—) and fitted curve (○) of aluminas obtained from thermal decomposition of bayerite (samples as described under Figure 1a). Horizontal lines including the abscissa axis are the zero-reflectance lines of each spectrum, which are all drawn to the same indicated scale. (b, bottom) Logarithm of the imaginary part of the dielectric constant deduced from fitting to experimental reflectance. Horizontal lines are the zero lines for the logarithm of the imaginary part of the relative dielectric constant for each curve.

NMR Spectroscopy. ^{27}Al MAS-NMR spectra were recorded at 104.26 MHz, with a Bruker MSL-400 spectrometer. The external magnetic field was 9.4 T. All measurements were carried out at 295 K, and the samples were spun around an axis

TABLE 1: Vibrational Parameters Obtained from Least-Squares Fit on Bayerite Series Reflectance Data

T (°C)	ω_T	γ_T	ω_L	γ_T	T (°C)	ω	γ	ω_L	γ_L
300					900	247.2	76.1	258.2	61.8
	310.0	245	438.9	112		281.0	53.1	299.9	64.6
	458.0	103	654.2	148		316.7	20.4	340.2	35.4
	592.8	111	550.8	370		356.3	23.3	375.2	45.2
	737.5	81.6	745.5	85.2		441.6	64.1	453.3	74.6
	786.8	308	937.6	87.1		505.5	56.6	549.1	68.4
$\epsilon_\infty = 4.13$				$R = 2.5\%$		564.9	60.2	590.0	51.9
						604.6	108	652.9	81.5
500	351.9	221	434.0	132		681.5	126	743.2	88.8
	482.3	109	670.1	269		766.0	35.3	770.4	31.3
	594.7	82.4	598.7	90.3		774.4	89.2	945.0	53.3
	736.8	79.2	740.1	82.1	$\epsilon_\infty = 3.44$				$R = 2.6\%$
	801.9	292	942.5	82.5					
$\epsilon_\infty = 3.15$				$R = 2.9\%$	1000	256.2	75.6	258.9	59.8
						282.4	57.0	297.0	54.8
700	322.5	150	363.7	49.4		317.9	21.7	343.0	30.8
	363.9	42.0	403.0	126		355.5	22.7	379.4	34.4
	487.2	122	655.1	254		441.4	54.3	451.5	63.0
	753.7	78.9	756.9	74.9		507.8	41.0	546.2	69.3
	791.9	300	947.4	50.1		566.1	56.8	589.8	45.4
$\epsilon_\infty = 3.36$				$R = 2.2\%$		603.6	104	652.5	70.1
						684.0	115	743.8	93.0
						767.0	31.6	772.3	30.6
800	313.5	117.3	356.5	45.2		785.4	80.7	945.7	36.6
	357.4	35.4	386.9	123	$\epsilon_\infty = 3.44$				$R = 2.6\%$
	496.7	111.8	640.2	209					
	768.2	72.7	770.6	62.3					
	778.2	264	946.4	48.4					
$\epsilon_\infty = 3.27$				$R = 3.3\%$					

inclined 54° 44′ with respect to the magnetic field, at a spinning rate of 12 kHz (MAS technique). NMR spectra were obtained after a $\pi/8$ excitation (2 μs) and intervals between successive accumulations of 5 s. Chemical shift values are given relative to an 1 M $AlCl_3$ aqueous solution. In all cases the mean error on position of the components was lower than 1 ppm. The sampling of the NMR signal was done with dwell times of 0.2 and 4 μs in order to analyze the whole spectrum (2.5 MHz) and the central transition (125 kHz). Special attention was given to properly choosing the origin of the FID signal (free induction decay) and to remove the points associated with the radiofrequency pulse, both necessary for a good determination of the baseline and phasing of NMR components. The baselines of the transformed spectra were finally corrected with a $\sin(kx)/kx$ expression to compensate for the lack of information in the neighborhood of the excitation pulse.

The analysis of ^{27}Al MAS-NMR spectra was done with the WINFIT[24] program. In this program, intensities of side bands are calculated with Herzfeld and Berger's method,[25] but quadrupolar C_Q and η constants must be determined by a trial and error procedure. In all cases, ^{27}Al MAS-NMR spectra were fitted by considering only first-order quadrupolar interactions, but in some favorable cases, quadrupolar constants were also estimated from the central transition shape ($^1/_2$, $-^1/_2$), by considering that second-order quadrupolar interactions were significant. In more disordered samples, a dispersion of electric field gradients produces a strong asymmetric broadening of the central ($^1/_2$, $-^1/_2$) transition. This asymmetric broadening was described by introducing two symmetric I_1 and I_2 components. From the fitted intensities of the two bands, a parameter of heterogeneity $h = I_2/(I_1 + I_2)$, was defined, where I_1 corresponds to the band centered at the maximum and I_2 to that which takes into account the upfield asymmetry. This parameter must be only considered as a qualitative guide due to the presence of second-order quadrupolar effects that have not been considered in this analysis.

Experimental Results

X-ray Diffraction. X-ray diffractograms have been used to identify the samples, following criteria established by Lippens and De Boer.[2] Diffraction patterns of samples obtained by heating bayerite are given in Figure 1a. In the diffractogram corresponding to 300 °C, narrow peaks of residual bayerite coexist with broad maxima of newly formed η-Al_2O_3. At 500 °C bayerite is eliminated altogether and the X-ray pattern corresponds to that of η-Al_2O_3 (see refs 1 and 2). Heating up to 800 °C does not substantially modify the diffractogram. However, at 900 °C, diffraction peaks narrow down, and a pattern similar to that of δ-Al_2O_3 previously reported[6] is obtained. At 1000 °C, the X-ray diffraction pattern corresponds to that of the θ-Al_2O_3 phase.[5,7] Finally, at 1100 °C corundum is formed (not shown).

The X-ray diffraction pattern of γ-Al_2O_3 is obtained by thermal treatment of boehmite during 2 h at 600 °C (Figure 1b). From 600 to 800 °C the XRD patterns do not change much, but above this temperature, δ-Al_2O_3 is clearly detected. Above 950 °C, variable proportions of θ- and α-phases in addition to δ-alumina were identified in diffractograms. From this temperature up to 1200 °C, prolonged thermal treatments increase the amount of α-Al_2O_3 at the expense of that of δ- and θ-Al_2O_3 phases. However, a short calcination of the γ-Al_2O_3 starting material (1200 °C during 6 min) gives a XRD pattern with a higher proportion of θ-Al_2O_3 (Figure 1b).

IR Reflectance Measurements. In order to keep a consistent notation for all samples, we have assumed that the vibrational spectra of transitional aluminas are assimilable to those of spinel[26] (space group $Fd\bar{3}m$). Under this assumption, the four detected modes will be identified as modes I to IV of the spinel structure. According to ab initio calculations of Ishii et al.,[27] these modes, in order of increasing frequency, correspond to I, stretching of octahedral against tetrahedral aluminum; II, bending of oxygen against aluminum ions; III, stretching of

anions against octahedral cations; and IV, stretching of anions against octahedral and tetrahedral cations.

The spectrum of the bayerite sample heated at 300 °C corresponds to a mixture of η-$Al_2O_3$11 with some remaining amount of bayerite, in good agreement with XRD observations. The IR reflectance spectrum presents the four expected bands (Figure 2a and Table 1) plus one additional band around 600 cm^{-1}, which is probably due to the presence of traces of bayerite. Small peaks due to the presence of OH^- groups were also found (see for example, the small feature around 1100 cm^{-1}). The imaginary part of the dielectric constant was fitted with 5 modes: modes I, III, and IV are located at 310, 737, and 787 cm^{-1} and mode II is split into two peaks at 458 and 593 cm^{-1} (Figure 2b). At 500 °C, the high-frequency peak of this doublet remains unchanged, while the low-frequency one, which is now clearly visible, shifts 24 cm^{-1} to higher frequencies, and mode I shifts up to 352 cm^{-1}. Hydroxyl groups are eliminated at 700 °C, and the mode around 600 cm^{-1} also vanishes. Above 700 °C, all bands narrow down and new small peaks are visible; in particular, a new band around 322 cm^{-1} is detected. These observations can be assigned (see the discussion below) to the onset of θ-Al_2O_3 formation. The new peaks gradually become better resolved up to 1000 °C, where the only phase detected by XRD is θ-Al_2O_3. For this phase the spectrum was fitted with a model of 11 oscillators (Table 1).

Spectra of transition aluminas obtained by calcination of boehmite (Figure 3 and Table 2) are similar to those obtained from bayerite. The resulting imaginary part of the dielectric constant deduced from reflectance IR data, plotted in Figure 3b, was adjusted with four modes at 371, 465, 776, and 819 cm^{-1} at 600 °C. At 700 °C, stretching bands corresponding to OH^- groups are eliminated (not shown). In samples heated at 800 °C the frequencies of modes I to III shift to lower values and, with the exception of mode II, the damping values decrease. From 900 to 950 °C, spinel modes start to split as a consequence of symmetry lowering. Upon further heating, peaks of the θ-Al_2O_3 phase are detected, and they are best resolved in the sample heated at 1200 °C for 6 min. In this sample as well as in that heated at 1000 °C, reflectance spectra were reproduced by using a 12-mode dielectric constant model, at least one (637 cm^{-1}) being a resolved mode of α-alumina. Finally, the spectrum of the sample heated at 1200 °C, 2 h shows the formation of α-Al_2O_3.

NMR Measurements. The ^{27}Al MAS-NMR spectra of the starting aluminas is formed by two broad asymmetric components placed around 70 and 0 ppm associated with tetra- and octahedral aluminum and their corresponding side bands. Central bands are asymmetrically broadened with respect to sidebands, suggesting that most of the Al atoms participate to the central lines; however, only part of them are detected in sidebands. The relative amounts of tetrahedral and octahedral Al were determined from the centerbands once subtracted the sideband intensities of the (5/2, 3/2) and (3/2, 1/2) transitions.[28]

The ^{27}Al MAS-NMR spectrum of η-Al_2O_3 phase, obtained by calcination of bayerite at 500 °C is formed by two components at 65 and 55 ppm (Figure 4a). Relative amounts of tetra- and octahedrally coordinated aluminum are respectively 28 and 72% (See Table 3). In samples heated at increasing temperatures, the octahedral component becomes narrower and the tetrahedral one broadens, increasing its integrated intensity. The full spectra of bayerite samples heated at different temperatures are given in Figure 4b. It is observed that the sideband pattern of octahedral aluminum spreads over a large spectral region and that the extent of its occupied region decreases with increasing temperature of treatment. On the contrary, the region covered by sidebands of tetrahedral aluminum slightly increases

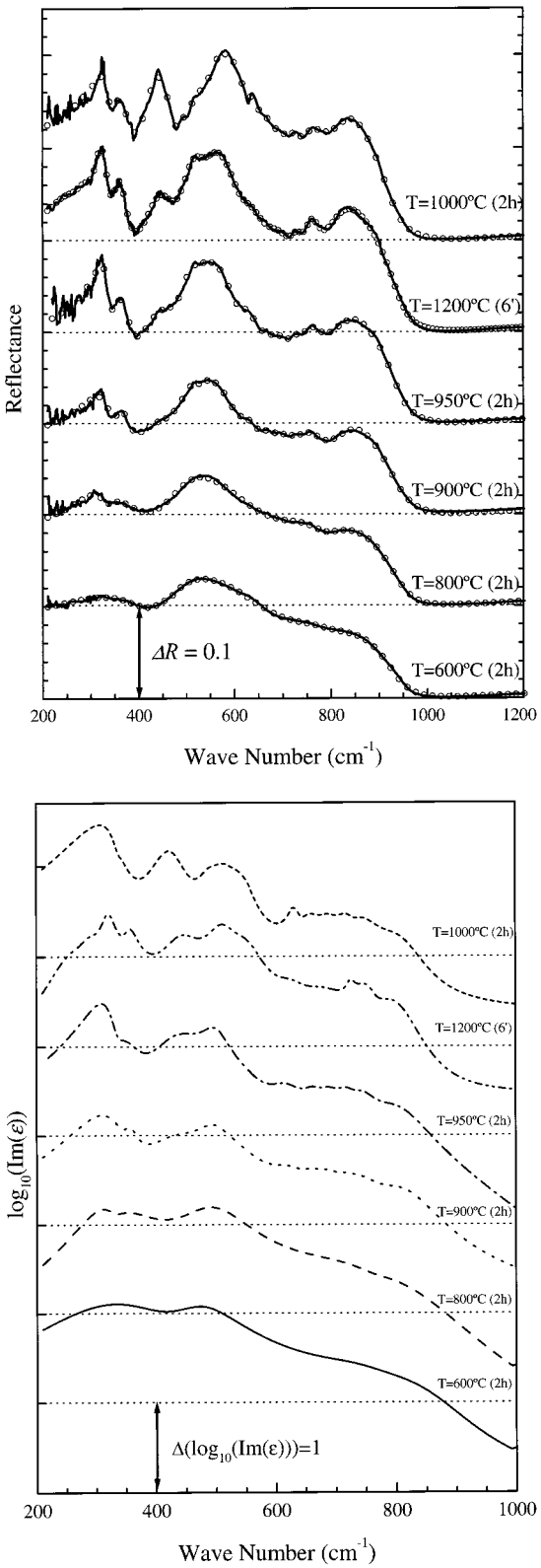

Figure 3. (a) (a, top) Experimental IR reflectance spectra (—) and fitted curve (○) of aluminas obtained from thermal decomposition of boehmite (samples as described under Figure 1a). Horizontal lines including the abscissa axis are the zero-reflectance lines of each spectrum, which are all drawn to the same indicated scale. (b, bottom) Logarithm of the imaginary part of the dielectric constant deduced from fitting to experimental reflectance. Horizontal lines are the zero lines for the logarithm of the imaginary part of the relative dielectric constant for each curve.

TABLE 2: Vibrational Parameters Obtained from Least-Squares Fit on Boehmite Series Reflectance Data

T (°C)	ω	γ	ω_L	γ_T
600	371.1	265	425.2	127
	464.9	137	712.2	296
	776.2	151	784.9	134
	819.1	231	940.9	77.5
$\epsilon_\infty = 3.39$				$R = 1.2\%$
800	331.2	62	332.3	47.4
	334.3	121	404.4	153
	497.6	126	663.5	308
	762.6	119	768.2	100
	804.6	262	948.7	67.6
$\epsilon_\infty = 3.3$				$R = 2.6\%$
900	329.6	96.2	349.6	28.3
	354.1	25.0	376.0	60.3
	447.6	117	462.4	82.1
	499.6	100	610.2	79.5
	525.3	57.7	525.7	49.3
	624.9	69.1	656.2	57.6
	665.4	38.8	674.1	40.8
	686.0	48.3	710.0	61.6
	721.9	31.6	724.1	34.5
	737.7	72.9	778.3	96.6
	812.3	115	948.2	73.5
$\epsilon_\infty = 3.4$				$R = 3.0\%$
950	331.5	63.3	339.4	21.7
	338.2	55.9	384.0	51.5
	439. 6	104.6	476.0	74.6
	502.1	60.8	605.7	66.2
	525.4	60.9	525.7	49.1
	618.8	64.5	656.5	55.0
	667.0	37.5	676.0	36.2
	686.1	43.6	704.5	53.7
	724.2	38.4	729.6	35.2
	739.0	67.3	778.3	75.9
	797.1	102	946.1	47.5
$\epsilon_\infty = 3.5$				$R = 3.6\%$
1200 (6′)	260.2	65.8	266.2	59.0
	290.3	55.4	303.5	50.5
	321.1	27.6	341.5	36.1
	357.6	27.6	376.7	55.0
	444.3	68.2	472.8	73.4
	510.5	54.6	538.4	72.7
	555.4	63.7	619.0	64.9
	627.5	58.6	659.5	84.2
	678.90	87.2	737.9	113.6
	724.7	16.4	724.1	21.5
	757.3	36.6	766.7	49.4
	802.9	88.5	945.0	52.7
$\epsilon_\infty = 3.34$				$R = 1.4\%$
1000	330.8	118	341.4	21.4
	337.9	34.1	384.9	51.9
	426.6	64.0	472.7	41.5
	492.8	33.2	496.0	32.2
	505.7	74.9	535.6	29.2
	536.9	29.6	640.3	42.9
	636.7	23.0	642.1	36.7
	656.4	43.6	683.9	43.2
	689.0	38.4	711.7	56.3
	723.2	33.6	730.4	35.8
	740.7	58.8	789.4	104
	811.8	95.0	934.7	57.0
$\epsilon_\infty = 3.45$				$R = 5.0\%$

with treatment temperature. From a fitting of sideband patterns, C_Q and η values were deduced and from these values, the isotropic chemical shifts were calculated (Table 3). It can be seen that the quadrupolar constant C_Q of tetrahedral aluminum slightly increases and that of octahedral aluminum appreciably decreases with increasing temperature. When θ-Al_2O_3 is formed, the intensities of tetrahedral and octahedral Al are approximately the same (47−53% at 1000 °C, see Table 3), and the quadrupolar constant of tetrahedral Al (5.5 MHz) is clearly higher than that of the octahedral one (3.1 MHz) (Figure 4b). At the same time, asymmetry η values of tetrahedral and octahedral aluminum are 0.8 and 0.4. In the case of the tetrahedral component of θ-Al_2O_3 phase, the shoulder at 65 ppm suggests the presence of second-order quadrupolar effects. The quadrupolar constants C_Q determined by fitting the centerbands is only a 10% higher than that deduced from fitting the sidebands pattern.

The ^{27}Al MAS-NMR spectra of γ-Al_2O_3 heated at increasing temperatures are given in Figure 5a. The spectrum at 600 °C is formed by two broad asymmetric components at 65 and 10 ppm, associated with Al in tetrahedral and octahedral coordination, and a small component at 30 ppm that is due to pentahedral Al (Figure 5a). The relative intensities of tetrahedral and octahedral components are 21 and 76%. When the sample is heated between 800 and 900 °C, the octahedral component becomes narrower and the tetrahedral one slightly broader. Above 950 °C, pentahedral aluminum is totally eliminated and the relative amount of tetrahedral aluminum increases. Finally, in the ^{27}Al MAS-NMR spectrum of the sample heated at 1000 °C, the amount of octahedral aluminum increases as a consequence of α-Al_2O_3 formation. From analysis of sidebands patterns (Table 3), it was concluded that C_Q of tetrahedral aluminum does not change very much above 900 °C, but that of the octahedral Al decreases clearly with temperature. In the spectrum of the sample heated at 1000 °C, the octahedral central line shifts toward more positive values and maxima of the α-Al_2O_3 phase are detected in the sideband pattern (Figure 5b, labeled with asterisks).

Discussion

In order to get information about the thermal evolution of transition aluminas, NMR, IR, and XRD techniques have been brought to bear. Information deduced from NMR spectra concerns aluminum coordination, but that obtained from IR spectroscopy refers to the atomic arrangement at the scale of a few unit cells. In the case of X-ray diffraction technique, a longer range order is required, and structural information refers to regions of several hundred angströms.

The thermal evolution of transition aluminas has two different stages, one extending up to 800 °C, and the second one from this point to 1000 °C. Above this temperature, transitional aluminas irreversibly transform into corundum in a broad temperature range from 1000 to 1200 °C.

Dehydroxylation of bayerite and boehmite proceeds in a similar way, only the temperatures are slightly different. Bayerite

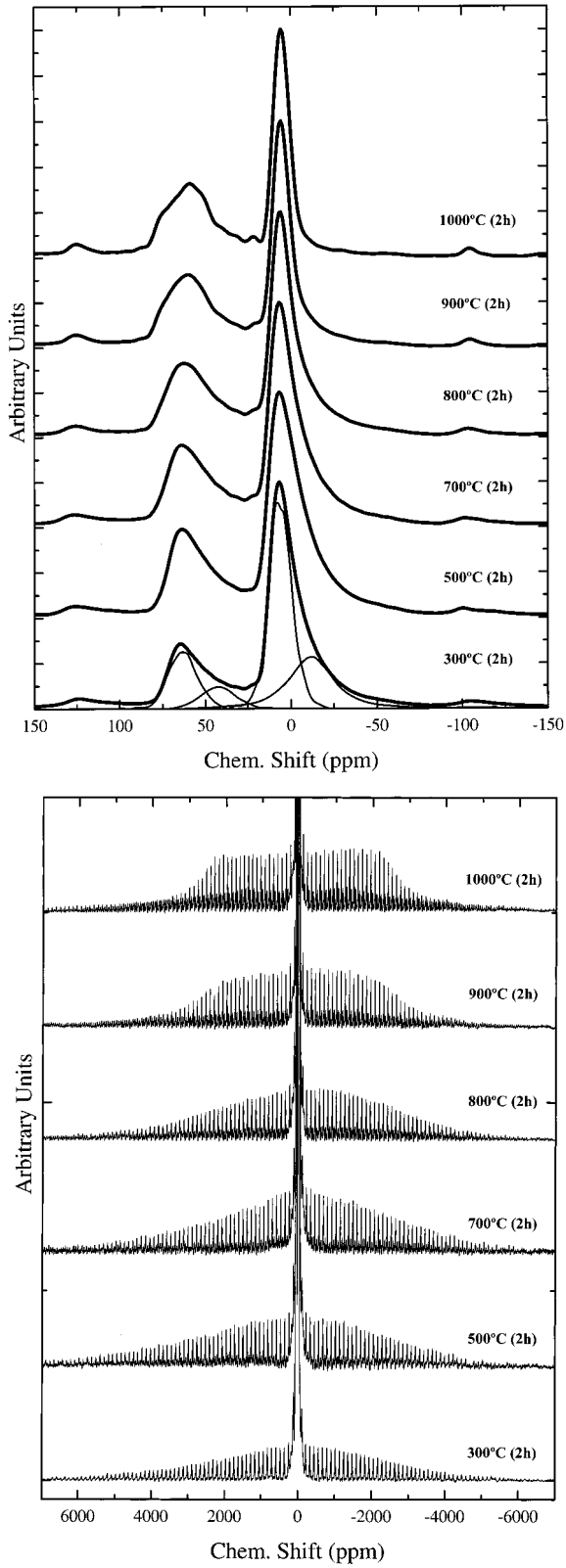

Figure 4. Evolution of (a, top) the central $-^1/_2,^1/_2$ transition and (b, bottom) the whole ^{27}Al MAS-NMR spectra of aluminas obtained from bayerite. Spectra were recorded at 12 kHz (samples as described under Figure 1a). In the case of the spectrum of the sample heated at 300 °C in (a), the symmetric components used on the fitting have been plotted.

heated at 500 °C is almost completely transformed into η-Al_2O_3 but total elimination of OH^- groups (they can be detected by a small band around 1100 cm^{-1}) and bayerite bands ($\omega = 592$ cm^{-1}) is only accomplished at 700 °C. The IR spectrum of bohemite heated at 600 °C (γ-Al_2O_3) also shows a small amount of OH^- groups and a small shoulder around 600 cm^{-1}, both precursor features that are also eliminated at 700 °C.

By separate study of the parameter γ_T deduced from fitting a model of oscillators to the reflectance spectra, it is possible to obtain information about the local order of the atoms which participate in each mode. Thus, the so-called "damping constant" of mode I mainly depends on short-range cationic order, while modes II, III, and IV also depend on the order of the oxygen sublattice. In addition, the damping of mode III only refers to octahedral disorder. The evolution of the damping constant with temperature is then a good order parameter. On the other hand, the heating process induces symmetry lowering and, as a consequence, the number of IR modes increases. High-temperature phases, δ- or θ-Al_2O_3, are structurally related with low temperature ones, η- and γ-Al_2O_3. Then the damping constants of all modes included in each $[\omega_{Tk}, \omega_{Lk}]$ interval, corresponding to a particular transverse-longitudinal splitting in the spinel structure, can be averaged because of their weak frequency dependence.[18,20] Thus, the averaged $\langle\gamma_{Tk}\rangle$ damping values of the components inside each spectral regions should only depend on the crystal order of the atoms involved in those vibrations. These values have been plotted in Figure 6 as a function of temperature. This parameter is very sensitive to structural order in the range 20−100 Å; in the case of large crystals, the values of γ_T are approximately 10 cm^{-1} (data for corundum can be found in refs 20 and 29), but in amorphous or disordered materials they can be one order of magnitude higher. The same analysis could be carried out on γ_L; however, this parameter strongly correlates with neighbor modes in the least square reflectance fit, and hence, has a larger error.

The analysis of damping values for both series of samples shows that those of modes II to IV remain nearly unchanged between 500 and 800 °C, but that of mode I suffers a continuous reduction with temperature. We think that this change corresponds to a cationic rearrangement inside the rigid skeleton of the fcc oxygen framework. This process occurs at lower temperatures in the bayerite than in the boehmite series.

In the ideal spinel structure the octahedral cations are twice as many as the tetrahedral ones, which gives relative proportions of 67−33% of octahedral and tetrahedral cations in this structure. In the defective spinel Al_2O_3, there is 1 Al missing for every 9 cations according to the formula $Al_8\square O_{12}$. If aluminum is preferentially located on octahedral sites as in a defect-free spinel, 75% (6/8) of the aluminum will be octahedral, while the remainder 25% will occupy tetrahedral positions, leaving $^1/_3$ of the spinel tetrahedral sites vacant. On the contrary, if aluminum fully occupies the tetrahedral positions of the ideal spinel, octahedral and tetrahedral aluminum will amount to 62.5 and 37.5% of the total. Usually, literature refers to these two cases as defective spinel structures with tetrahedral or octahedral vacancies. In the case of η-Al_2O_3 at 300 °C, 78% of aluminum cations are in octahedral coordination while at 700 °C, once the dehydroxylation process has finished, only 69% of them remain in octahedral positions (Table 3 and Figure 7). These values indicate a mixed character between the above two spinel types, so that it appears that cationic defects could be equally distributed between octahedral and tetrahedral positions.[1,3] On the contrary, the NMR spectrum of γ-Al_2O_3 exhibits three peaks (Figure 5), which correspond to octahedral, pentahedral, and tetrahedral coordination of aluminum. At 600 °C, the occupation of the different sites are 76, 3, and 21%, respectively (Table 3 and Figure 7). These values agree with a model of preferential location of vacancies at tetrahedral sites. In this sample there exists a significant proportion of pentahedral aluminum[30,31] (3−

TABLE 3: NMR Parameters of Bayerite and Boehmite Series[a]

(A) Bayerite Series

T (°C)	δ_{Tet} (ppm)	δ_{Oct} (ppm)	C_Q^{Tet} (MHz)	C_Q^{Oct} (MHz)	η_{Tet}	η_{Oct}	I_{Tet} (%)	I_{Oct} (%)	h_{Tet} (%)	h_{Oct} (%)
300	77.5	15.1	4.7	3.9	0.7	0.4	22	78	29	45
500	76.5	14.5	4.5	3.9	0.7	0.4	28	72	35	50
700	77.3	14.2	4.9	3.8	0.5	0.4	31	69	33	50
800	79	15	5.2	4.0	0.5	0.4	33	67	31	45
900	80	11	5.5	3.0	0.5	0.4	43	57	20	32
1000	80	11.3	5.5	3.1	0.8	0.4	47	53	4	18

(B) Boehmite Series

T (°C)	δ_{Tet} (ppm)	δ_{Oct} (ppm)	C_Q^{Tet} (MHz)	C_Q^{Oct} (MHz)	η_{Tet}	η_{Oct}	I_{Tet} (%)	I_{Pent} (%)	I_{Oct} (%)	h_{Tet} (%)	h_{Oct} (%)
600	78.3	14	4.9	3.7	0.7	0.4	21	3	76	30	33
800	78.5	15.2	4.7	3.6	0.7	0.4	24	6.5	69	35	40
900	77.7	13.5	4.7	3.7	0.7	0.4	26	4	70	33	44
950	77	14	5.1	3.3	0.7	0.4	37	3	60	30	45
1200[b]	79	12.2	5.5	3.0	0.7	0.4	37	0	62	15	25
1000	74	14	5.3	3.1	0.7	0.4	25	0	75	12	15

[a] The estimated errors on δ are 0.7 ppm. and those on C_Q and η values are 0.2 MHz and 0.1, respectively. Relative errors on integrated intensities are 5% while those for h parameters are 10%. [b] 6 minutes.

6.5%), which is probably due to aluminum atoms at the surface of the particles. This analysis differs considerably from those previously reported[3,12] on spectra recorded with a lower spinning rate (4 kHz), in which detection of pentahedral and tetrahedral components was hindered by the presence of octahedral sidebands. Similar conclusions were deduced by Slade et al.[32] during the study of thermal transformation of alumina hydrates. On the other hand, we see no hint of any abnormal aluminum coordination in NMR spectra of η-alumina, contrary to reports by Zhou and Snyder.[4] Quadrupolar constants associated with the two main types of aluminum coordination in γ- and η-Al_2O_3 phases are similar (Figure 8). The quadrupolar constants, C_Q are significantly different from zero, which would indicate a clear departure from the ideal cubic symmetry. Quadrupolar constants are larger for tetrahedra ($C_Q = 4.7-4.9$ MHz) than they are for octahedra ($C_Q = 3.6-3.9$ MHz). Similar conclusions were obtained by Kunath-Fandrei et al.;[33] however, in that case, the C_Q constants were slightly higher (5 and 4.5 MHz, respectively). Additionally, deduced asymmetry values, η, are different from zero, suggesting that the symmetry at Al sites may be lower than axial (Table 3). As a consequence of the structural disorder, central components ($-^1/_2/^1/_2$ transitions) are very asymmetric. Although it could be possible to perform an analysis of the asymmetric broadening of centerbands by assuming sites with different quadrupolar constants,[33,34] the existence in this case of several possible solutions with different distributions of C_Q and η made us to desist from using this procedure. In order to describe the asymmetry of these components, only two bands were finally introduced and the parameter h described in the experimental section has been adopted. This parameter, related to Al-site heterogeneity, is approximately 40% for octahedra (Figure 10), but it takes on a value around 30% for the tetrahedral component in both fases.

From 800 to 1000 °C, large changes have been observed by IR and NMR spectroscopies, as well as by X-ray diffraction. In this range of temperatures, the evolution of structural parameters in both series of samples notably differs. In the first case, the transformation of η-Al_2O_3 into θ-Al_2O_3 is a gradual process. The XRD pattern of the sample heated at 800 °C corresponds to that of η-Al_2O_3, but at 900 °C it notably changes displaying at 1000 °C the pattern of θ-Al_2O_3. In these samples, narrow bands are observed in reflectance spectra corresponding to the IR spectrum of θ-Al_2O_3, which is fully developed at 900 °C. This experimental spectrum displays 11 out of the 12 bands predicted by group theory (Table 1).

$$\Gamma_{vib} = \underbrace{10A_g + 5B_g}_{\text{Raman}} + \underbrace{4A_u + 8B_u}_{\text{IR}}$$

The average damping constant for each spinel mode decreases for modes II and IV around 800 °C while the already low value of mode I only slightly diminishes. The damping constant of mode III does not change over the whole range of temperatures (Figure 6). These data can be explained through the increase of long-range order in the oxygen sublattice that goes parallel to textural changes detected by TEM. It should be noted that the X-ray diffraction peaks only start to narrow at 900 °C, i.e. 100 °C above the temperature detected by IR. This could mean that from 800 to 900 °C the crystallite size would be of the order of some tens of angströms.

From 800 to 1000 °C, octahedral and tetrahedral aluminum fractions tend toward the theoretical limit of 50−50% which corresponds to θ-Al_2O_3 (53−47% at 1000 °C). The thermal evolution of C_Q for tetrahedral aluminum consists of a gradual increase toward 5.7 MHz, while for octahedral aluminum, a steep decrease from 4 to 3 MHz happens near 900 °C. Based on these facts, the heating of bayerite samples produces higher distortions in tetrahedra and lower distortions in octahedra. In θ-Al_2O_3 heated at 1000 °C, (Table 3) the chemical shift values, corrected for second-order quadrupolar effects, are respectively 80 and 11.3 ppm. for tetrahedral and octahedral coordination of aluminum. These observations indicate the formation of a well-defined phase (θ-Al_2O_3) that is difficult to detect when lower spinning rates are used, because the presence of tetra- and octahedral side bands in the analyzed spectral region. In this phase, quadrupolar constants are 5.5 and 3.1 MHz. respectively, indicating that tetrahedra and octahedra are considerably distorted. An analysis of distortions of polyhedra is difficult because of the different influence of O−Al−O angles and Al−O distances in C_Q constants. In general, a modification on the shorter Al−O tetrahedral distances should affect more the C_Q constants than that produced in the longer octahedral distances. This fact has been experimentally confirmed.

In a similar way as in η-Al_2O_3, the process of heating γ-Al_2O_3 samples at temperatures higher than 800 °C also produces a notable increase in order. In Figure 6 it can be observed that the damping constants of modes II and IV behave in the same way as in the bayerite series. However, at 900 °C, neither the X-ray pattern nor the IR spectrum shows any sign of formation

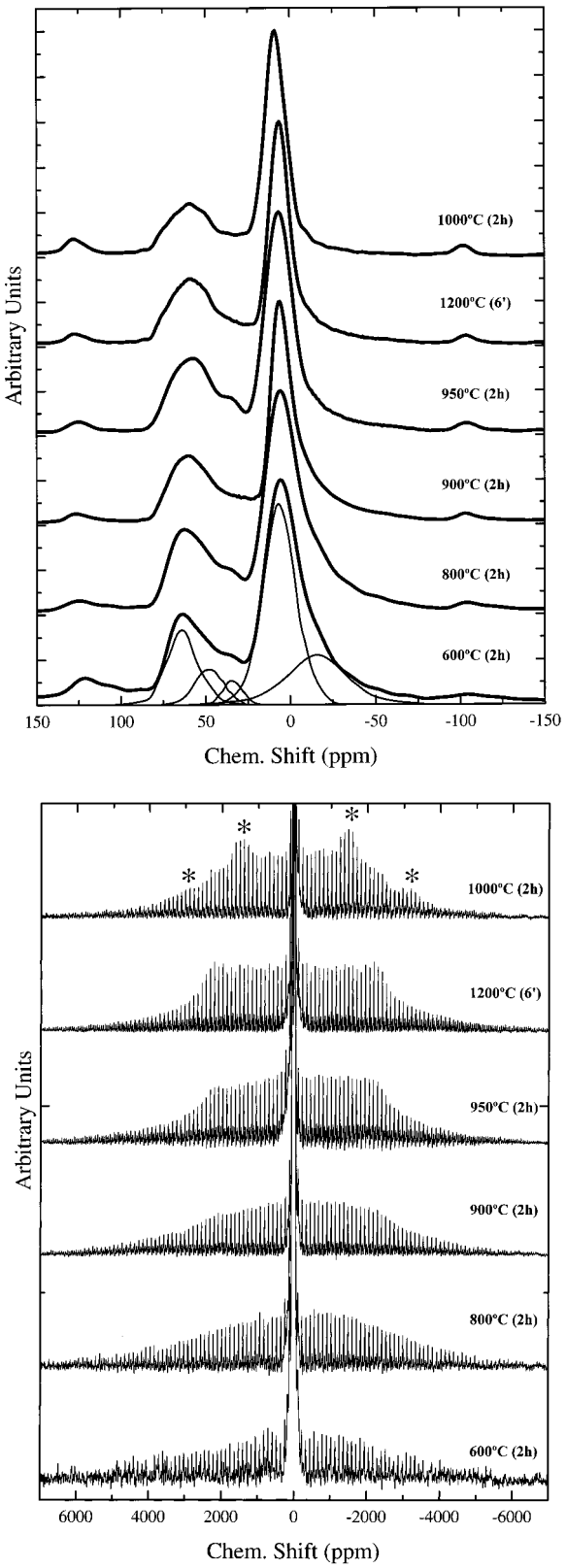

Figure 5. Evolution of (a, top) the central $-1/2,1/2$ transition and (b) the whole ^{27}Al MAS-NMR spectra of aluminas obtained from boehmite. Spectra were recorded at 12 kHz (samples as described under Figure 1b). In the case of the spectrum of the sample heated at 600 °C in the (a), the symmetric components used on the fitting have been plotted.

of a lower symmetry phase. Furthermore, the sample heated at 950 °C presents an X-ray pattern similar to that of δ-Al_2O_3 reported in the literature[2,6] with small amounts of θ-Al_2O_3. By

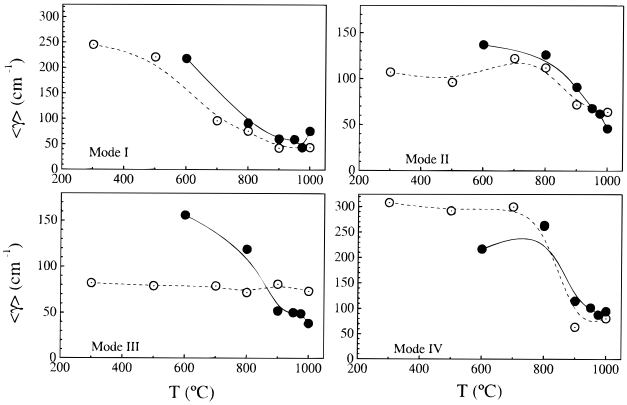

Figure 6. Damping of vibrational modes of alumina samples obtained from thermal decomposition of bayerite (○) and bohemite (●).

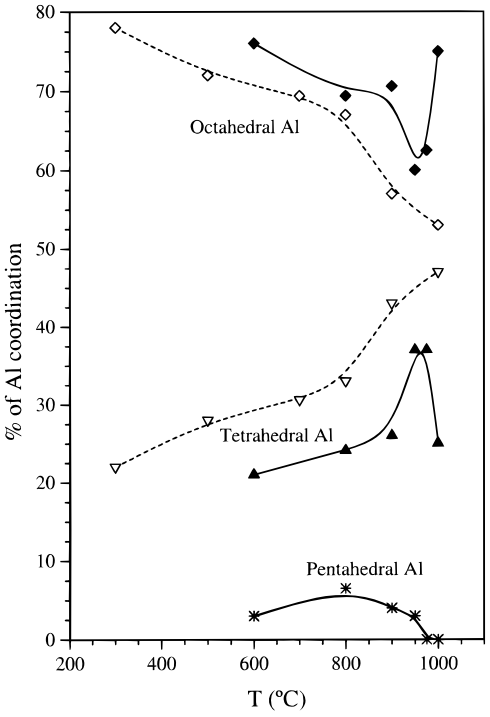

Figure 7. Temperature evolution of structural sites occupancies deduced from the intensity of the central band of ^{27}Al NMR spectra of calcined aluminas. Open symbols stand for bayerite series and the full ones for that of boehmite. Diamonds (◇) stand for octahedral aluminum, triangles (▽) for tetrahedral aluminum, and stars (*) for pentahedral aluminum.

using the triple spinel cell of δ-Al_2O_3,[6] group theory analysis predicts the existence of 104 IR modes:

$$\Gamma_{vib} = 40A_1 + 42B_1 + \underbrace{40A_2}_{\text{Raman}} + \underbrace{41B_2}_{\text{IR}} + \underbrace{63E}_{\text{Raman,IR}}$$

Experimental spectra only show 11 modes at frequencies very close to those of γ- and θ-Al_2O_3. Taking into account that for a similar material, γ-Fe_2O_3, in which the triple cell has been proved correct by different diffraction techniques,[35,36] up to 28 modes were clearly observed,[37] it must be concluded that the IR spectrum of this sample does not agree with the hypothesis of a trebled spinel cell. Instead, the IR reflectance spectrum can be explained as a mixture of γ- and θ-Al_2O_3. NMR data also confirms this hypothesis. C_Q and chemical shift values are similar to those of γ-Al_2O_3 in the 600−900 °C temperature range (see Table 3). In this range of temperature, the occupancy ratio

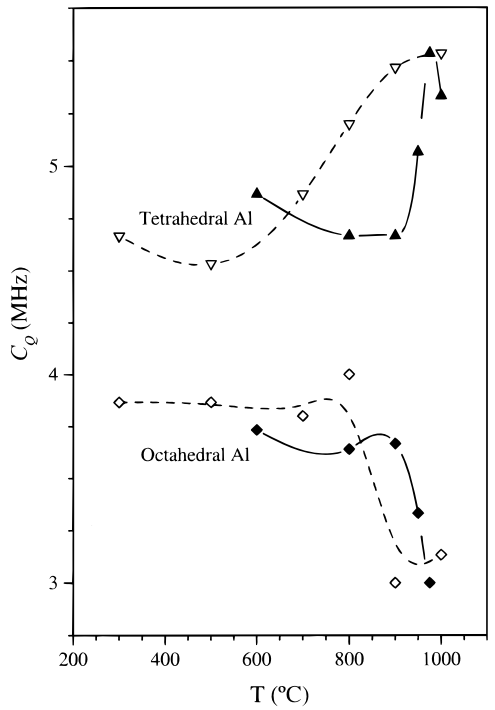

Figure 8. Temperature evolution of C_Q deduced from ^{27}Al NMR sideband patterns of calcined aluminas. Labeling is the same as Figure 7.

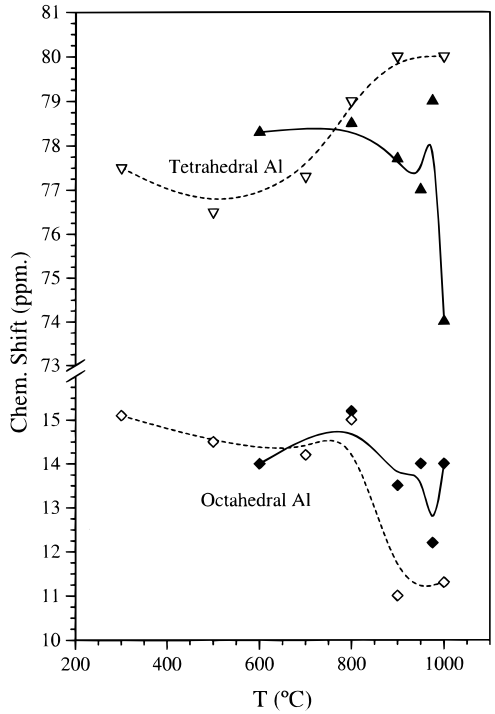

Figure 9. Temperature evolution of chemical shift of ^{27}Al MAS-NMR components. Positions were corrected for second-order quadrupolar shifts. Labeling is the same as Figure 7.

of octahedral, tetrahedral, and pentahedral aluminum does not notably change. At the same time, the asymmetry broadening of the NMR components, the *h* parameters, reach maxima of 45% and 33% at 950 °C. This suggests that at this temperature considerable amounts of γ-Al_2O_3 transform into θ-Al_2O_3 in such a way that the material can be seen as a binary mixture. This is also confirmed by close observation of C_Q, chemical shift and Al coordination. All these magnitudes have intermediate values between those of γ- and θ-Al_2O_3. It should be remarked that at

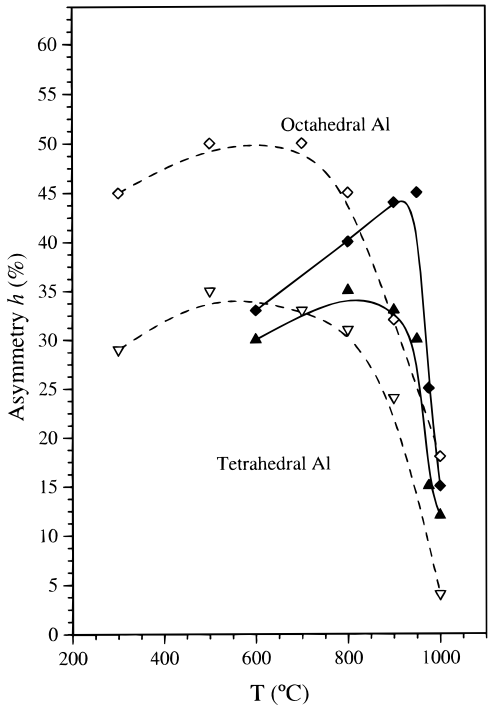

Figure 10. Temperature evolution of the heterogeneity parameter deduced from the shape of the central $-^1/_2,^1/_2$ transition of ^{27}Al MAS-NMR spectra of calcined aluminas. Labeling is the same as in Figure 7.

950 °C most of pentahedral aluminum has been eliminated. It is well-known that the addition of defects, as sodium cations,[2,4] stabilizes the spinel structure of γ-Al_2O_3, even at temperatures as high as 1100 °C. We think that in this case, pentahedral aluminum, probably located at crystallite surfaces, could play the same role in γ-Al_2O_3. When the temperature is sufficiently high, aluminum defects become unstable and cations rearrange to form θ-Al_2O_3. The presence of pentahedral aluminum in γ-Al_2O_3 could also be responsible for the strong catalytic activity as compared to that of η-Al_2O_3. Finally, the sample heated at 1200 °C for only 6 min, where pentahedral aluminum was also removed, presents IR, XRD, and NMR parameters very similar to those of θ-Al_2O_3.

α-Al_2O_3 formed by a process of nucleation and growth of the oxygen sublattice begins to appear, in the boehmite series, at temperatures higher than 950 °C, in such a way that in the sample heated at 1000 °C for 2 h, three alumina phases, γ-, θ-, and α-Al_2O_3, can be detected by XRD, IR, and NMR. The formation of θ-Al_2O_3 and corundum in the temperature range from 900 to 1200 °C follows kinetics with different time constants, so that in a short thermal process, the θ phase tends to form, while in case of long firing times corundum is always obtained.[10] When α-Al_2O_3 is formed, chemical shift values and quadrupolar constants of octahedral Al components tend toward those of corundum ($\delta_{iso} = 16$ ppm, and $C_Q \sim 2.38$ MHz);[38] and η vanishes, which is typical of axial symmetry.

Conclusions

From the IR and NMR analysis of samples obtained from thermal decomposition of boehmite and bayerite, new insights on the structural characteristics of transitional aluminas, defined by their XRD patterns, have been obtained.

From bayerite dehydroxylation, η-Al_2O_3 is formed in which aluminum vacancies are randomly distributed over spinel octahedral and tetrahedral sites. The transition from η- to

θ-Al_2O_3 occurs in two steps: from 300 to 800 °C, only ordering of cations is detected, while above 800 °C, all atoms participate in θ-Al_2O_3 formation. The structure of θ-Al_2O_3 is made of distorted octahedra and tetrahedra in proportions close to 1:1. Distortion of the Al coordination polyhedra is the origin of quadrupolar constants measured for tetrahedra (5.5 MHz) and octahedra (3.1 MHz).

In γ-Al_2O_3 formed from boehmite, cation vacancies are preferentially located at tetrahedral sites and 5% of Al is pentahedrally coordinated; we assume these atoms to be at the particle surface, and responsible for the origin of the catalytic activity of this phase. In addition, all experimental evidence points to thermal stabilization of γ-Al_2O_3 by structural defects at the crystallite surfaces that are eliminated above 900 °C. Spectral features of a trebled cell, similar to that found in γ-Fe_2O_3, have not been found in samples characterized as δ-Al_2O_3. On the other hand, an important degree of heterogeneity has been deduced from NMR and IR data in that sample, which seems to be constituted by a mixture of the well crystallized phases, γ- and θ-Al_2O_3, instead of a single δ-Al_2O_3 phase. In samples heated between 900−1200 °C, θ-Al_2O_3 formation competes with that of corundum, and δ, θ, and α phases can be found, in variable proportions, in a wide range of temperatures. Above 1000 °C, corundum is the only stable phase.

Acknowledgment. We acknowledge financial support of DGICYT (Spain) through Research Project PB 95-0225, and thank S. Medioroz and J. C. Conesa for kindly furnishing the precursor samples used in this work.

References and Notes

(1) Wefers, K.; Misra, C. *Oxides and Hydroxides of Aluminum*; Alcoa Technical Paper No. 19; Revised: Alcoa Laboratories: Pittsburgh, PA, 1987.
(2) Lippens, B.C.; de Boer, J.H. *Acta Crystallogr.* **1964**, *17*, 1312.
(3) John, C. S.; Alma, V. C. M.; Hays, G. R. *Appl. Catal.* **1983**, *6*, 341.
(4) Zhou, R. S.; Snyder, R. L. *Acta Crystallogr.* **1991**, *B47*, 617.
(5) Yamaguchi, G.; Yasui, I.; Chiu, W. C. *Bull Chem. Soc. Jpn.* **1970**, *43*, 2487.
(6) Repelin, Y.; Husson, E. *Mater. Res. Bull.* **1990**, *25*, 611.
(7) Husson, E.; Repelin, Y. *Eur. J. Solid State Inorg. Chem.* **1996**, *33*, 1223.
(8) Megaw, H.D. *Crystal Structures;* W.B. Saunders Co.: Philadelphia, PA, 1973; p 221.
(9) Greenwood, N.N. *Ionic Crystals Lattice Defects and NonStoichiometry*; Butterworths: London, 1970; p 92.
(10) Wilson, S. J.; McConnell, J. D. C. *J. Solid State Chem.* **1980**, *34*, 315.
(11) Pecharromán, C; González-Carreño, T.; Iglesias, J. E. *J. Mater. Res.* **1996**, *11*, 127.
(12) Urretavizcaya, G.; Cavalieri, A. L.; Porto López, J.; Sobrados, I.; Sanz, J. J. *Mater. Synth. Processing* **1998**, *6*, 1.
(13) Landauer, R. *J. Appl. Phys.* **1952**, *23*, 779.
(14) Landauer, R. In *Proceedings of the Fist Conference on the Electrical Transport and Optical Properties of Inhomogeneous media*; Garland, J.C., Tanner, D.B., Eds.; AIP Conf. Proc. No. 40; AIP: New York, 1978; p 2.
(15) Pecharromán, C.; Iglesias, J. E. *Phys. Rev.* **1994**, *B49*, 7137.
(16) Pecharromán, C.; Iglesias, J. E. *J. Phys. Condens, Matter* **1994**, *6*, 7125.
(17) Osborn, J. A. *Phys. Rev.* **1945**, *67*, 351.
(18) Baker A. S. *Phys. Rev. A* **1964**, *136*, 1290.
(19) Gervais, F.; Piriou, B. *Phys. Rev. B* **1974**, *10*, 1642.
(20) Gervais, F.; Piriou, B. *J. Phys. C* **1974,** *7*, 2374.
(21) Bohren, C. F.; Huffman, D. R. *Absorption and Scattering of Light by Small Particles*; John Wiley and Sons: New York, 1983; pp 367−369.
(22) Fuchs, R. *Phys. Rev. B* **1978,** *18*, 7160.
(23) Genzel, L.; Martin, T. P. *Phys. Stat. Solidi (B)* **1972**, *51*, 91.
(24) Massiot, D. *WINFIT Programme*; Bruker-Franzen Analytic Gmbh: Berlin, 1993.
(25) Herzfeld, J.; Berger, E. *J. Chem. Phys.* **1980**, *73*, 6021.
(26) White, W. B.; De Angelis, B. A. *Spectrochim. Acta* **1967**, *23a*, 895.
(27) Ishii, M.; Nakahira, M.; Yamanaka, T. Solid State Commun. **1972**, *11*, 209.
(28) Massiot, D.; Bessada, C.; Coutures J.P.; Taulelle F. *J. Magn. Reson.* **1990**, *90*, 231.
(29) Barker, A. S. *Phys. Rev.* **1963**, *132*, 1474.
(30) Alemany, L. B.; Kirker, G. W. *J. Am. Chem. Soc.* **1986**, *108*, 6158.
(31) Sanz, J.; Sobrados, I.; Cavalieri, A. L.; Pena, P.; de Aza, S.; Moya, J. S. *J. Am. Ceram. Soc.* **1991**, *74*, 2398.
(32) Slade, R. C. T; Southern J. C.; Thompson I. M.; *J. Mater. Chem.* **1991,** *1*, 563.
(33) Kunath-Fandrei, G.; Bastow, T. J.; Hall, J. S.; Jäger, C.; Smith, M. E. *J. Phys. Chem.* **1995**, *99*, 15138.
(34) Kraus, H.; Müller, M.; Prins R.; Kentgens, A.P.M. *J. Phys. Chem.* **1998,** *102*, 3862.
(35) Boudelle, M.; Batis-Landoulsi, H.; Leclercq, Ch.; Vergnon, P. *J. Solid State Chem.* **1983**, *48*, 21.
(36) Greaves, C. *J. Solid State Chem.* **1983**, *49*, 325.
(37) Pecharromán, C.; González-Carreño, T.; Iglesias, *J. E. Phys. Chem. Miner.* **1995**, *22*, 21.
(38) Jakobsen, H. J.; Skibsted, J.; Bildsøe, H.; Nielsen, N. C. J. Magn. *Reson.* **1989**, *85*, 173.